

Optical chirality induced by spin-orbit interaction of light in a tightly focused Laguerre-Gaussian beam

Mingchao Zhu(朱明超), Shenggui Fu(付圣贵), and Zhongsheng Man(满忠胜)
Citation: Chin. Phys. B, 2023, 32 (**11**): 114202. DOI: 10.1088/1674-1056/acefc9
Journal homepage: http://cpb.iphy.ac.cn; http://iopscience.iop.org/cpb

What follows is a list of articles you may be interested in

Tightly focused properties of a partially coherent radially polarized power-exponent-phase vortex beam

Kang Chen(陈康), Zhi-Yuan Ma(马志远), and You-You Hu(胡友友)
Chin. Phys. B, 2023, 32 (**2**): 024208. DOI: 10.1088/1674-1056/ac70b0

Variable optical chirality in atomic assisted microcavity

Hao Zhang(张浩), Wen-Xiu Li (李文秀), Peng Han(韩鹏), Xiao-Yang Chang(常晓阳), Shuo Jiang(蒋硕), An-Ping Huang(黄安平), and Zhi-Song Xiao(肖志松)
Chin. Phys. B, 2020, 29 (**11**): 114207. DOI: 10.1088/1674-1056/abb660

Three-dimensional modulations on the states of polarization of light fields

Peng Li(李鹏), Dongjing Wu(吴东京), Sheng Liu(刘圣), Yi Zhang(章毅), Xuyue Guo(郭旭岳), Shuxia Qi(齐淑霞), Yu Li(李渝), Jianlin Zhao(赵建林)
Chin. Phys. B, 2018, 27 (**11**): 114201. DOI: 10.1088/1674-1056/27/11/114201

Tight focusing of axially symmetric polarized vortex beams

Zhou Zhe-Hai (周哲海), Guo Yang-Kuan (郭阳宽), Zhu Lian-Qing (祝连庆)
Chin. Phys. B, 2014, 23 (**4**): 044201. DOI: 10.1088/1674-1056/23/4/044201

Experimental verification on tightly focused radially polarized vortex beams

Du Fu-Rong (杜富荣), Zhou Zhe-Hai (周哲海), Tan Qiao-Feng (谭峭峰), Yang Chang-Xi (杨昌喜), Zhang Xiao-Qing (张晓青), Zhu Lian-Qing (祝连庆)
Chin. Phys. B, 2013, 22 (**6**): 064202. DOI: 10.1088/1674-1056/22/6/064202

Optical chirality induced by spin–orbit interaction of light in a tightly focused Laguerre–Gaussian beam

Mingchao Zhu(朱明超)[1], Shenggui Fu(付圣贵)[1], and Zhongsheng Man(满忠胜)[1,2,†]

[1] *School of Physics and Optoelectronic Engineering, Shandong University of Technology, Zibo* 255000, *China*
[2] *Collaborative Innovation Center of Light Manipulations and Application, Shandong Normal University, Jinan* 250358, *China*

(Received 21 June 2023; revised manuscript received 31 July 2023; accepted manuscript online 14 August 2023)

Optical chirality is one of the important and fundamental dynamic properties of light besides energy, momentum, and angular momentum. The quantification of electromagnetic chirality has been conceptualized only recently. Now, it is well known that for paraxial plane waves of light, the optical chirality is proportional to the ellipticity of the polarization ellipse, i.e., completely independent of the phase distribution. Here it is shown that optical vortex and state of polarization of the source paraxial field both have contributions to the optical chirality of the nonparaxial field generated by tightly focused Laguerre–Gaussian (LG) beam, which is in Stark contrast to the paraxial plane wave of light known from classical optics. The physical reason is the redistribution of local electromagnetic polarization in three dimensions associated with spin–orbit interaction.

Keywords: tight focusing, optical chirality, spin–orbit interaction

PACS: 42.25.Fx, 11.30.Rd, 67.30.hj, 71.70.Ej **DOI:** 10.1088/1674-1056/acefc9

1. Introduction

Chirality describes the mirror symmetry violation that an object cannot superimpose with its own mirror image through rotation and translation.[1] Chiral objects are prevalent in nature and can be directly judged from their geometry; in other word, geometric chirality is essentially a non-local three-dimensional (3D) structural property of an object that requires a non-vanishing spatial extent. In addition, geometric chirality is a qualitative binary property.[2,3] Electromagnetic fields also have chirality,[4–25] which, by contrast, can be measured quantitatively. Optical rotatory dispersion and circular dichroism are two typically measured chiroptical phenomena. The quantification of the chirality of electromagnetic fields has been conceptualized only recently as optical chirality,[4] also known as Lipkin's 00-Zilch, discovered decades ago.[26] It is important to emphasize that light generally exhibits chirality through circular polarization, a localized property where electric and magnetic field vectors take on a helical shape as they propagate. Therefore, optical chirality in the traditional sense cannot describe any form of chirality originating from the spatial extent of the beam. Most recently, due to the global properties of polarization and phase structure, a new type of chirality, called Kelvin's chirality, has been proposed.[21]

With the development of modern nano-optics and photonics, non-paraxial 3D structured light fields have attracted much attention due to their fascinating properties compared to paraxial light. A key difference between paraxial two-dimensional (2D) plane wave and non-paraxial 3D structured light is that, in addition to the usually dominant transverse field, the latter also has a significant longitudinal component oriented along the direction of propagation. This leads to many extraordinary properties of non-paraxial fields, such as transverse spin angular momentum (SAM).[27–38] It is well known that SAM is closely related to optical helicity through the continuity equation.[39–41] Furthermore, the optical helicity is proportional to the optical chirality of the monochromatic field.[5] In addition, the optical field can also carry orbital angular momentum (OAM) through optical vortices.[42] Also, spin–orbit interactions have been demonstrated including, but not limited to, beam focusing through aplanatic objectives,[43,44] scattering through small particles,[45,46] excitation and scattering of surface plasmon polaritons,[47,48] and transmission through nanoapertures.[49,50] However, the effect of the interaction between the source optical vortex and helicity on the chirality in the tightly focused non-paraxial 3D structured fields is not fully understood.

In this paper, we systematically study the role and contribution of the optical degree of freedom including optical vortices and states of polarization (SoPs) of the source paraxial field on the optical chirality density of the nonparaxial field generated by tightly focused Laguerre–Gaussian beams. To this end, using Richards and Wolf vectorial diffraction method, the explicit expressions to calculate the strength vector of the 3D electric and magnetic fields are presented. The results show that the optical chirality of highly confined 3D structured field is significantly richer than that of the 2D paraxial plane wave. In addition, the structures and appearances of chirality density distributions mainly depend on the interaction between topological charge and ellipticity. Orientation, how-

†Corresponding author. E-mail: zsman@sdut.edu.cn
© 2023 Chinese Physical Society and IOP Publishing Ltd

ever, nearly has no effect on the chirality density distribution. The physical cause is the redistribution of the local electromagnetic polarization in 3D space associated with spin–orbit interactions.

2. Theoretical model

In paraxial 2D light, it is well known that the optical helicity is proportional to the degree of elliptical polarization: zero for linearly polarized and unpolarized light fields, and a maximum for circularly polarized light.[51] For a monochromatic paraxial source field of arbitrary ellipticity, its SoP can be described by the combination by a pair of orthogonal right- and left-handed circularly polarized basis, $|R\rangle$ and $|L\rangle$. Here we adopt a unit vector $|U\rangle$ to describes the polarization state, as follows:[52–57]

$$|U\rangle = a_R|R\rangle + a_L|L\rangle, \tag{1}$$

where the orthonormal circular polarization basis are

$$|R\rangle = \frac{1}{\sqrt{2}}(\hat{e}_x - \mathrm{i}\hat{e}_y), \tag{2}$$

$$|L\rangle = \frac{1}{\sqrt{2}}(\hat{e}_x + \mathrm{i}\hat{e}_y). \tag{3}$$

a_R and a_L in Eq. (1) are complex coefficients indicating the fraction between the two bases. If the intensity is normalized, a_R and a_L can be expressed as follows:

$$a_R = \cos\sigma - \exp(-\mathrm{i}\phi_0), \tag{4}$$

$$a_L = \sin\sigma \exp(+\mathrm{i}\phi_0), \tag{5}$$

where $\sigma \in [0, \pi/2]$ determines the fraction and ϕ_0 is the additional relative phase between the two bases. And the ellipticity of the polarization ellipse can be derived as

$$\varepsilon = \tan\left(\sigma - \frac{\pi}{4}\right). \tag{6}$$

Normalized Stokes parameters (SPs) in the circular basis of Eqs. (1)–(5) are given by

$$S_0 = |\langle R|\,U\rangle|^2 + |\langle L|\,U\rangle|^2 = 1, \tag{7}$$

$$S_1 = 2\,\mathrm{Re}\left(\langle R|\,U\rangle^*\langle L|\,U\rangle\right) = \sin 2\sigma\cos 2\phi_0, \tag{8}$$

$$S_2 = 2\,\mathrm{Im}\left(\langle R|\,U\rangle^*\langle L|\,U\rangle\right) = \sin 2\sigma\sin 2\phi_0, \tag{9}$$

$$S_3 = |\langle R|\,U\rangle|^2 - |\langle L|\,U\rangle|^2 = \cos 2\sigma. \tag{10}$$

S_1, S_2, and S_3 may be regarded as the sphere's Cartesian coordinates of a point on a unit Poincaré sphere (PS) as shown in Fig. 1, where S_0 is the radius of the PS.[58] This point can also be described by the latitude 2Θ and longitude 2Φ, and their relationships are

$$\sin 2\Theta = S_3/S_0, \tag{11}$$

$$\tan 2\Phi = S_2/S_1. \tag{12}$$

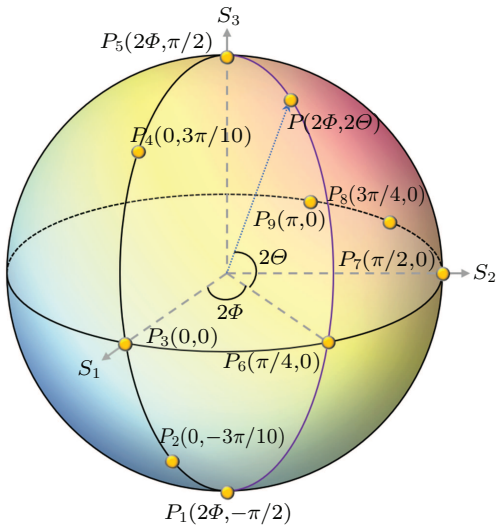


Fig. 1. Poincaryé sphere representation of all possible polarization states of a monochromatic paraxial source field.

Based on Eqs. (7)–(12), we can obtain the correspondence between the parameters that determine the polarization distribution of the source beam and the coordinates on the PS

$$2\sigma = \frac{\pi}{2} - 2\Theta, \tag{13}$$

$$2\phi_0 = 2\Phi. \tag{14}$$

Theoretically, the optical chirality density of a monochromatic light field can be expressed as[4,26]

$$\chi = \frac{1}{2}(\boldsymbol{E}\cdot\nabla\times\boldsymbol{E} + \mu\boldsymbol{H}\cdot\nabla\times\boldsymbol{H}), \tag{15}$$

where ν and μ are the permittivity and permeability respectively, and $\boldsymbol{E}$ and $\boldsymbol{H}$ are the real electric and magnetic fields in the time domain. Performing time averaging, the time-averaged optical chirality density can be obtained as follows:

$$\langle\chi\rangle = \frac{\omega}{2\upsilon^2}\,\mathrm{Im}(\boldsymbol{e}\cdot\boldsymbol{h}^*), \tag{16}$$

where ω and υ represent the angular frequency and the speed of light, respectively, and $\boldsymbol{e}$ and $\boldsymbol{h}$ are the complex amplitude vectors of the electric and magnetic fields in the spatial domain; here, superscript asterisk indicates complex conjugation. Non-paraxial 3D structured light fields can be obtained in an aplanatic high numerical aperture (NA) objective focusing system. When the polarization distribution of the incident field is represented by Eq. (1), the corresponding 3D electromagnetic fields $\boldsymbol{e}$ and $\boldsymbol{h}$ for any point $P(\rho_P, \varphi_P, z_P)$ in the image space can be obtained using Richard–Wolf vectorial diffraction theory[59]

$$\begin{bmatrix}\boldsymbol{e}\\ \boldsymbol{h}\end{bmatrix} = -\frac{\mathrm{i}kf}{2\pi}\int_0^{\alpha}\int_0^{2\pi}\sqrt{\cos\theta}A(\theta)\begin{bmatrix}\boldsymbol{v}_\mathrm{e}\\ \boldsymbol{v}_\mathrm{h}\end{bmatrix} \times \mathrm{e}^{\{\mathrm{i}k[-\rho_P\sin\theta\cos(\phi-\varphi_P)+z_P\cos\theta]\}}\sin\theta\,\mathrm{d}\phi\,\mathrm{d}\theta, \tag{17}$$

where k and f are the wave number in the image space and focal length of the focusing objective lens, respectively; $\alpha = \arcsin(\mathrm{NA}/n)$, where NA is the numerical aperture and

n is the index of refraction in the image space; ϕ and θ denote, respectively, the azimuthal angle with respect to x axis in the objective space and tangential angle with respect to z axis. To reveal the optical chirality induced by interactions between source optical vortex and helicity, we employ an incident field with a Laguerre–Gaussian $\mathrm{LG}_{(l,p)}$ complex amplitude distribution, where l and p are the numbers of intertwined helices known as the topological charge and additional concentric rings. With $p=0$, the function $A(\theta)$ is given by[60]

$$A(\theta)=\left(\frac{\sqrt{2}\beta\sin\theta}{\sin\alpha}\right)^{|l|}\exp\left(-\frac{\beta^2\sin^2\theta}{\sin^2\alpha}\right)\exp(\mathrm{i}l\phi), \quad (18)$$

where β is the ratio of the pupil radius to the beam waist.

In Eq. (17), $\boldsymbol{v}_\mathrm{e}$ and $\boldsymbol{v}_\mathrm{h}$ represent the electric and magnetic field polarization vectors in image space contributed by the input SoP; their three mutually perpendicular components v_{ex}, v_{ey}, and v_{ez} as well as v_{hx}, v_{hy}, and v_{hz} are found to be

$$\begin{aligned}
v_{ex} &= c_1\left(\sin^2\phi+\cos^2\phi\cos\theta\right)\\
&\quad +c_2\sin\phi\cos\phi\left(\cos\theta-1\right), \quad (19)\\
v_{ey} &= c_1\sin\phi\cos\phi\left(\cos\theta-1\right)\\
&\quad +c_2\left(\sin^2\phi\cos\theta+\cos^2\phi\right), \quad (20)\\
v_{ez} &= c_1\cos\phi\sin\theta+c_2\sin\phi\sin\theta, \quad (21)\\
v_{hx} &= \sqrt{\frac{\nu}{\mu}}[c_1\sin\phi\cos\phi\left(\cos\theta-1\right)\\
&\quad -c_2\left(\cos^2\phi\cos\theta+\sin^2\phi\right)], \quad (22)\\
v_{hy} &= \sqrt{\frac{\nu}{\mu}}[c_1\left(\sin^2\phi\cos\theta+\cos^2\phi\right)\\
&\quad -c_2\sin\phi\cos\phi\left(\cos\theta-1\right)], \quad (23)\\
v_{hz} &= \sqrt{\frac{\nu}{\mu}}\left(c_1\sin\theta\sin\phi-c_2\sin\theta\cos\phi\right), \quad (24)
\end{aligned}$$

where c_1 and c_2 are as follows:

$$c_1=\frac{\sqrt{2}}{2}\left[\cos\sigma\exp(-\mathrm{i}\phi_0)+\sin\sigma\exp(\mathrm{i}\phi_0)\right], \quad (25)$$

$$c_2=\frac{\sqrt{2}\mathrm{i}}{2}\left[\sin\sigma\exp(\mathrm{i}\phi_0)-\cos\sigma\exp(-\mathrm{i}\phi_0)\right]. \quad (26)$$

Based on the above equations, we can now study the optical chirality caused by the interaction between optical vortex and helicity of the input 2D paraxial field in focused non-paraxial 3D structured light fields. All length measurements are in units of wavelength of the input field, $\beta=1.5$, NA $=1.2$, $n=1.33$, and $f=2$ mm are used in the following calculations.

3. Optical chirality in the non-paraxial 3D focused field

In revealing the chirality of the tightly focused optical field caused by the interaction of helicity (local nature) and vorticity (spatial nature) of the incident optical field, it is first necessary to clarify the chirality density of the focused optical field when there is no spin in the incident optical field. To this end, we select five LG input fields with topological charge $l=1$ and polarization states at P_3, P_6, P_7, P_8, and P_9 on PS in Fig. 1 as examples to study the corresponding optical chirality density distribution in the focused light field. All these input fields are linearly polarized, but have different orientations, as shown in the first row in Fig. 2. From the second row in Fig. 2, we can see that for all the different input fields, the optical chirality density distributions show almost the same patterns. When $p=0$, they are two different rings with different signs, and the chiral density on optical axis is obtained in the case of $l=1$. Moreover, the magnitude of the optical chiral density of the outer ring is much smaller than that of the inner ring. Therefore, the orientation, as an important adjustable polarizable degree of freedom of the incident optical field, seems to have no effect on the chirality of the focused 3D field.

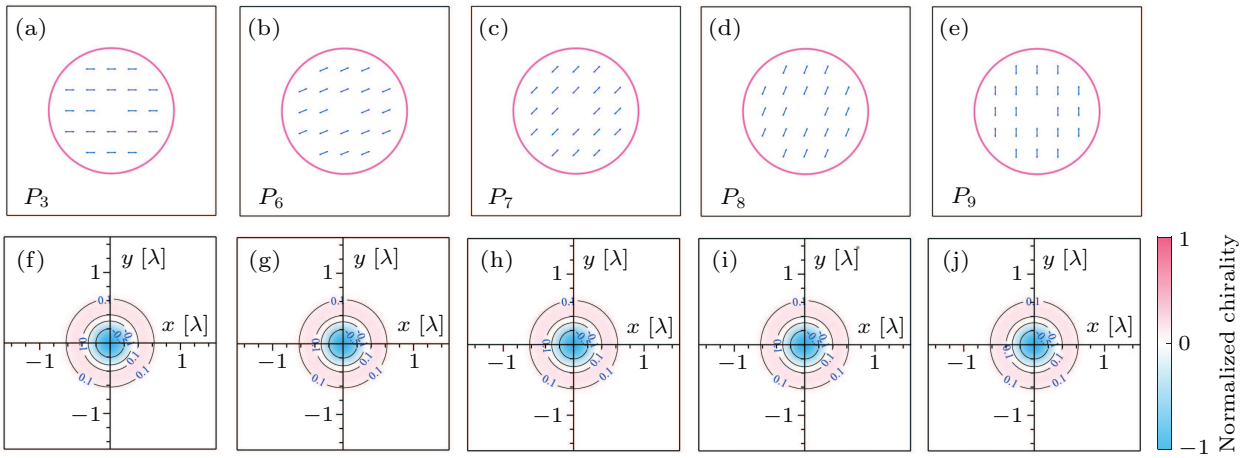


Fig. 2. Polarization distributions of five $\mathrm{LG}_{(1,0)}$ input fields with polarization states located at the points P_3, P_6, P_7, P_8, and P_9 on the PS (upper row) and the corresponding optical chirality density distributions in the focal plane (lower row). All distributions of the optical chirality density are normalized to their common maximum.

The above results confirm the chiral character of the 3D focused fields of the input beams carrying OAM, even if these beams are linearly polarized and therefore have no SAM. Figure 3 shows the effect of the sign and size of the pseudo-scalar topological charge l on the chiral density distribution, where the five LG input fields have the same polarization state located at P_3 on the PS, and differ only in the topological charge l. It is clear that there is no chiral density distribution when $l = 0$ [see Fig. 3(c)], which further suggests that the chirality of the tightly focused field is contributed by the OAM of the incident field. Then as $|l|$ continues to increase, the optical chiral density always exhibits a centrally symmetric ring structure and the sign reverses in the radius direction. In addition, the radius of the annular optical chiral density increases. The difference is apparent when the sign of the topological charge changes, i.e., regions of high chirality in the focal plane are replaced by regions of opposite chirality density, and vice versa. Therefore, when the input field has no SAM, the structure and appearance of the chirality density distribution depends entirely on the topological charge, i.e., the polarization orientation has no effect on the chirality.

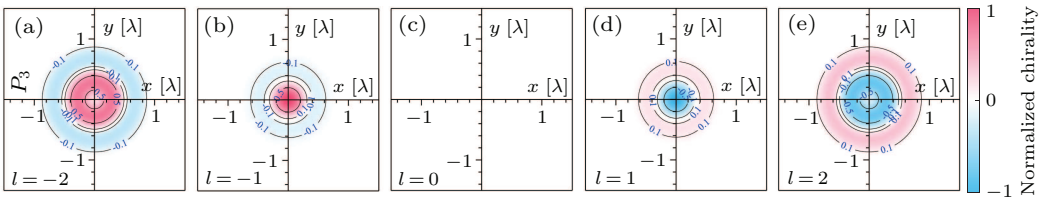


Fig. 3. Theory-derived optical chirality density distributions in the focal plane of five different LG input fields with polarization states located at the point P_3 (the incident beams are linearly polarized light) on the PS and topological charges $l = -2$, -1, 1, and 2, respectively. All distributions of the optical chirality density are normalized to their common maximum.

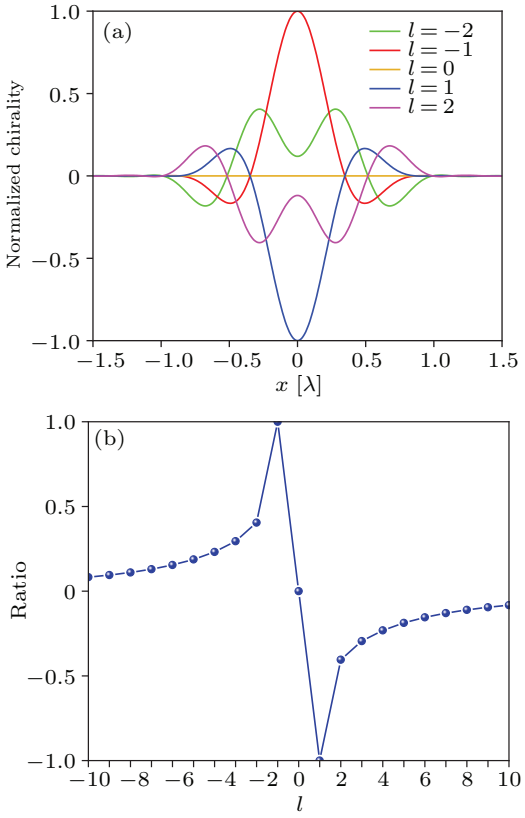


Fig. 4. (a) Optical chirality density profiles along x axis in the focal plane of the same five LG input fields as in Fig. 3. All distributions of the optical chirality density are normalized to their common maximum. (b) Ratio of the peak optical chirality density of each incident light field in the focal plane to the common maximum of their absolute values versus the topological charge l.

The magnitude of the optical chirality density is another important parameter in the interaction of chiral optical fields with matter. To gain more insight into the OAM-induced optical chirality shown in Figs. 2 and 3, we now explore the effect of the topological charge l on the magnitude of optical chirality. Figure 4(a) shows the optical chirality distributions along the x axis in the focal plane for the same five LG input fields as in Fig. 3. All the optical chirality density distributions are normalized to their common maximum. It is clear that the peak of the optical chiral density varies considerably with the topological charge l. The specific trend is shown in Fig. 4(b), which depicts the ratio of the peak optical chiral density for each incident light field in the focal plane to the common maximum of the optical chiral density for different incident light fields with respect to the topological charge. Obviously, when choosing $l = 1$ and -1, we can obtain the highest chirality for the input linearly polarized LG beam.

For any point on the PS moving from the north pole toward the equator and then to the south pole along a fixed meridian, the ellipticity of the polarization ellipse varies from -1 to 0 and then to 1, the handedness changes from right-handed to left-handed, but the orientations remain the same. As examples, we choose five different $\mathrm{LG}_{(1,0)}$ input fields with SoPs located at points P_5, P_4, P_3, P_2, and P_1 on the PS [see Fig. 1] to explore the effect of spin–orbital interaction on the optical chirality density distribution in the 3D focused field [see Fig. 5]. The optical chirality density changes significantly in structure and appearance. Specifically, when the input field does not carry SAM, it is two rings with different signs [see Fig. 5(c)]. In contrast, when the input ellipticity is nonzero, a pattern of only one loop appears [see Figs. 5(a), 5(b), 5(d), and 5(e)]. Here, it seems that both the local handedness of the input elliptical polarization and the global handedness of the optical vortex have an effect on the sign of the optical chirality.

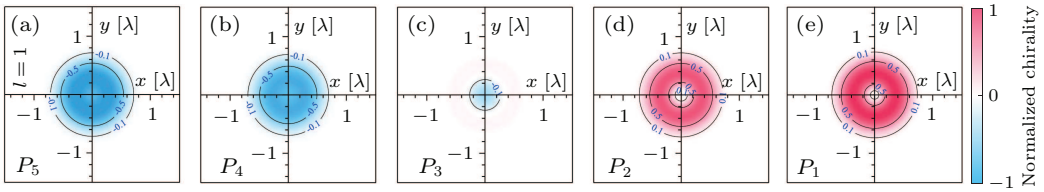


Fig. 5. Theory-derived optical chirality density distributions in the focal plane of five different $LG_{(1,0)}$ input fields with polarization states located at the points P_1, P_2, P_3, P_4, and P_5 on the PS, respectively. All distributions of the optical chirality density are normalized to their common maximum.

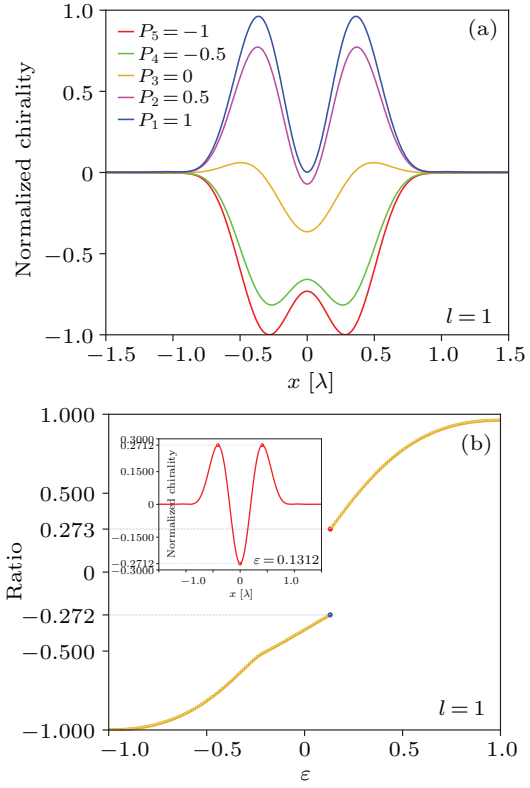


Fig. 6. (a) Optical chirality density profiles along x axis in the focal plane of the same five LG input fields as shown in Fig. 5. All distributions of the optical chirality density are normalized to their common maximum. (b) The ratio of the peak chiral density of each incident optical field in the focal plane to the common maximum of their absolute values versus the input ellipticity ε.

To better understand the effect of spin–orbit interactions on the optical chirality, figure 6(a) shows the optical chirality density distribution along the x axis in the focal plane of the same five LG input fields as shown in Fig. 5. All the optical chirality density distributions are normalized to the common maximum of their absolute values. It is clear that the peak of the chiral density varies accordingly with the input ellipticity. Most importantly, whether the chiral density lies on or off the optical axis can be controlled simply by a suitable ellipticity value. The effect of ellipticity on the magnitude of chiral density is shown in Fig. 6(b), from which we can see that the relational curve is clearly a segmented function. By calculations, the threshold position is found at about $\varepsilon = 0.1312$, its corresponding optical chirality density profile along x axis can be seen in the inset in Fig. 6(b). Under this condition, the chirality at the position of the optical axis is equal in magnitude and opposite in sign to the chirality around it. On both sides of this threshold position, the sign of the peak chiral density is opposite.

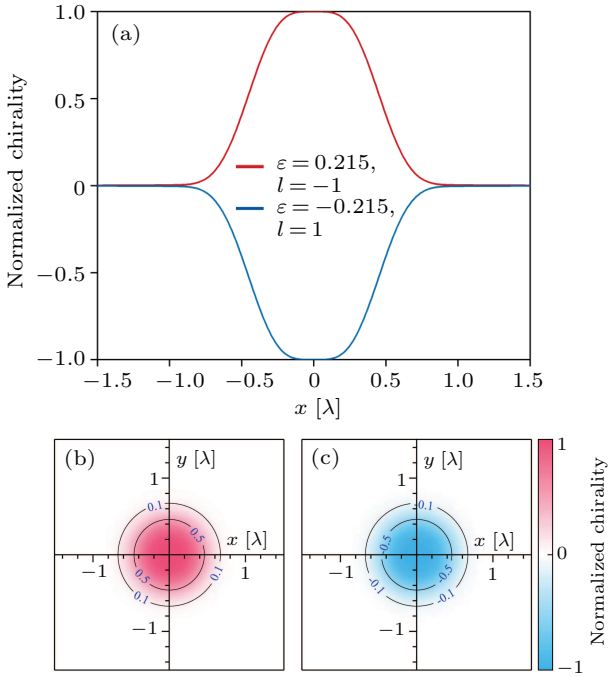


Fig. 7. (a) Flat-topped optical chirality density profiles along x axis in the focal plane of two LG input fields with $(\varepsilon, l) = (0.215, -1)$ and $(-0.215, 1)$, respectively. (b) and (c) The corresponding optical chirality density distributions in the focal plane. The distributions of these two optical chirality densities are normalized to their common maximum.

Light fields with uniform optical chirality may be useful and scarce in practical applications. Fortunately, by carefully selecting the ellipticity and topological charge of the input field, the flat-topped optical chiral density distribution can be obtained, as shown in Fig. 7. Obviously, the chirality of the light field can be freely switched only by the signs of ellipticity and topological charge. In addition, the structure and appearance of the chiral density distribution remain unchanged, which may be very useful for comparing the reflection of chiral substances under different chiral light fields. The above peculiar chiral distribution originates from the polarization distribution of local electric and magnetic fields. Figure 8 shows the corresponding electric and magnetic field polarization distributions in the focal plane and their projections onto the three orthogonal planes. In general, all polarization distributions are extremely complex, because the polarization projections on the x–y and y–z planes become solid ellipses in some regions,

indicating that the rotation axes of the electric and magnetic fields are no longer parallel to the z axis; that is to say, due to the existence of the longitudinal component,[43,44] the local polarization ellipse is not in the plane parallel to the x–y plane. For the polarization projection on the x–y planes become solid ellipses in some regions, indicating that the rotation axes of the electric and magnetic fields are no longer parallel to the z axis; that is to say, due to the existence of the longitudinal component,[43,44] the local polarization ellipse is not in the plane parallel to the x–y plane. For the polarization projection on the x–y plane, we can see those regions of right-handedness when $(\varepsilon, l) = (0.215, -1)$ are replaced by left-handedness when $(\varepsilon, l) = (-0.215, 1)$, for both electric and magnetic fields, and *vise versa*. As a result, optical fields with opposite chirality can be obtained while the structure and appearance are maintained.

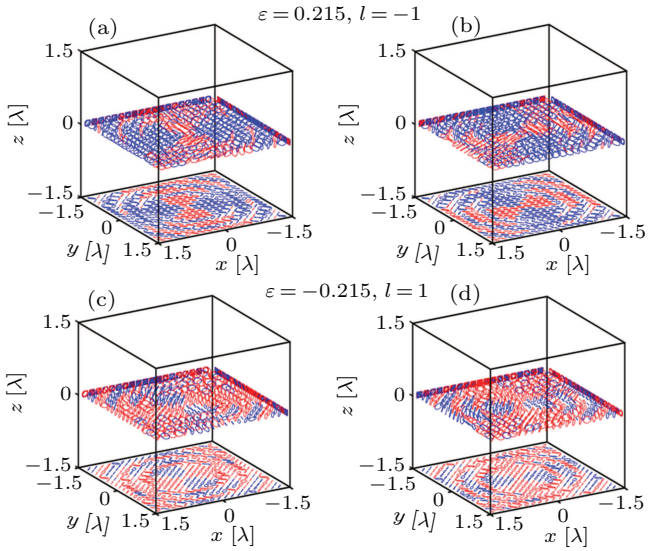


Fig. 8. Theoretically calculated electric and magnetic field polarization distributions in the focal plane and their projections onto the three orthogonal planes of tightly focused two LG fields with $(\varepsilon, l) = (0.215, -1)$ (upper row) and $(-0.215, 1)$ (lower row), respectively. Panels (a) and (c) depict the electric field polarization distributions, while panels (b) and (d) depict the magnetic field polarization distributions. Red and blue indicate that the local polarization ellipses are right-handed and left-handed, respectively.

4. Conclusions

In summary, we have studied the contributions of optical vortices and SoP of the source 2D paraxial light field on the chirality density distributions of 3D nonparaxial structured field in tight focusing. To this end, we have taken LG input field that has arbitrary SoP as an example and uses the Richards and Wolf vectorial diffraction method to derive the corresponding explicit expressions to calculate the strength vector of the 3D electric and magnetic fields. The results show that the optical chirality of highly confined 3D structured light field is obviously richer than that of the 2D paraxial plane wave. Both optical vortex and SoP of the source paraxial field have contributions to the optical chirality of the nonparaxial field, which is in stark contrast to the paraxial plane wave in classical optics. But, the structures and appearances of chirality density distributions mainly depend on the interaction between the topological charge and the ellipticity. Orientation, however, has almost no effect on the chirality density distribution. The physical origin is the redistribution of the local electromagnetic polarization in 3D space associated with spin–orbit interactions. These findings may be of help in chiral particle trapping and nanoscale chiral detection and sensing.

Data availability statement

The data that support the findings of the present study are openly available in the Science Data Bank at https://doi.org/10.57760/sciencedb.j00113.00162.

Acknowledgements

Project supported by the National Natural Science Foundation of China (Grant No. 12074224) and the Natural Science Foundation of Shandong Province, China (Grant Nos. ZR2021YQ02 and ZR2020MA087).

References

[1] Barron L D 2012 *Chirality* **24** 879
[2] Efrati E and Irvine W T M 2014 *Phys. Rev. X* **4** 011003
[3] Fernandez-Corbaton I, Fruhnert M and Rockstuhl C 2016 *Phys. Rev. X* **6** 031013
[4] Tang Y and Cohen A E 2010 *Phys. Rev. Lett.* **104** 163901
[5] Bliokh K Y and Nori F 2011 *Phys. Rev. A* **83** 021803
[6] Schäferling M, Dregely D, Hentschel M and Giessen H 2012 *Phys. Rev. X* **2** 031010
[7] Coles M and Andrews D L 2012 *Phys. Rev. A* **85** 063810
[8] Gorodetski Y, Drezet A, Genet C and Ebbesen T W 2013 *Phys. Rev. Lett.* **110** 203906
[9] Ding K, Ng J, Zhou L and Chan C T 2014 *Phys. Rev. A* **89** 063825
[10] Vázquez-Lozano J E and Martínez A 2018 *Phys. Rev. Lett.* **121** 043901
[11] Yang D, Li Y, Deng D, Chen Q, Zhang Y, Liu Y, Gao J and Sun M 2018 *Opt. Lett.* **43** 4594
[12] Forbes K A and Andrews D L 2018 *Opt. Lett.* **43** 435
[13] Hu H, Gan Q and Zhan Q 2019 *Phys. Rev. Lett.* **122** 223901
[14] Machinnon N 2019 *J. Opt.* **21** 125402
[15] Mun J, Kim M, Yang Y, Badloe T, Ni J, Chen Y, Qiu C and Rho J 2020 *Light: Sci. & Appl.* **9** 139
[16] Li M, Yan S, Zhang Y and Yao B 2020 *Nanoscale* **12** 15453
[17] Yang D, Li C, Yao Z, Huang X, Li Y, Jin P and Lin J 2020 *Phys. Rev. Appl.* **14** 014066
[18] Zhu T, Shi Y, Ding W, Tsai D P, Cao T, Liu A Q, Nieto-Vesperinas M, Sáenz J J, Wu P C and Qiu C 2020 *Phys. Rev. Lett.* **125** 043901
[19] Forbes K A and Jones G A 2021 *J. Opt.* **23** 115401
[20] Koksal K, Babiker M, Lembessis V E and Yuan J 2021 *Opt. Commun.* **490** 126907
[21] Nechayev S, Eismann J S, Alaee R, Karimi E, Boyd R W and Banzer P 2021 *Phys. Rev. A* **103** L031501
[22] Chen W, Yang Q, Chen Y and Liu W 2021 *Phys. Rev. Lett.* **126** 253901
[23] Forbes K A and Andrews D L 2021 *J. Phys. Photon.* **3** 022007
[24] Forbes K A and Jones G A 2021 *Phys. Rev. A* **103** 053515
[25] Zhu M, Fu S and Man Z 2022 *Optik* **262** 169278
[26] Lipkin D 1964 *J. Math. Phys.* **5** 696
[27] Bliokh K Y, Bekshaev A Y and Nori F 2014 *Nat. Commun.* **5** 3300
[28] Aiello A, Banzer P, Neugebauer M and Leuchs G 2015 *Nat. Photon.* **9** 789
[29] Neugebauer M, Bauer T, Aiello A and Banzer P 2015 *Phys. Rev. Lett.* **114** 063901

[30] Bauer T, Neugebauer M, Leuchs G and Banzer P 2016 *Phys. Rev. Lett.* **117** 013601
[31] Neugebauer M, Eismann J S, Bauer T and Banzer P 2018 *Phys. Rev. X* **8** 021042
[32] Pan Y, Gao X, Zhang G, Li Y, Tu C and Wang H 2019 *APL Photon.* **4** 096102
[33] Meng P, Man Z, Konijnenberg A P and Urbach H P 2019 *Opt. Express* **27** 35336
[34] Zhang S, Fu S, Zhang H, Ge X, Bai Z, Lyu Y, Zhao R and Man Z 2019 *Opt. Express* **27** 33621
[35] Man Z, Dou X and Urbach H P 2020 *Opt. Commun.* **458** 124790
[36] Eismann J S, Nicholls L H, Roth D J, Alonso M A, Banzer P, Rodríguez-Fortuño F J, Zayats A V, Nori F and Bliokh K Y 2021 *Nat. Photon.* **15** 156
[37] Zhang X, Shen B, Zhu Z, Rui G, He J, Cui Y and Gu B 2020 *Opt. Express* **30** 5121
[38] Man Z, Zhang Y and Fu S 2022 *Opt. Express* **30** 31298
[39] Cameron R P, Barnett S M and Yao A M 2012 *New J. Phys.* **14** 053050
[40] Barnett S M, Cameron R P and Yao A M 2012 *Phys. Rev. A* **86** 013845
[41] Bliokh K Y, Bekshaev A Y and Nori F 2013 *New J. Phys.* **15** 033026
[42] Allen L, Beijersbergen M W, Spreeuw R J C and Woerdman J P 1992 *Phys. Rev. A* **45** 8185
[43] Zhao Y, Edgar J S, Jeffries G D M, McGloin D and Chiu D T 2007 *Phys. Rev. Lett.* **99** 073901
[44] Man Z, Xi Z, Yuan X, Burge R E and Urbach H P 2020 *Phys. Rev. Lett.* **124** 103901
[45] Bliokh K Y, Ostrovskaya E A, Alonso M A, Rodríguez-Herrera O G, Lara D and Dainty C 2011 *Opt. Express* **19** 26132
[46] Haefner D, Sukhov S and Dogariu A 2009 *Phys. Rev. Lett.* **102** 123903
[47] Gorodetski Y, Niv A, Kleiner V and Hasman E 2008 *Phys. Rev. Lett.* **101** 043903
[48] O'Connor D, Ginzburg P, Rodríguez-Fortuño F J, Wurtz G A and Zayats A V 2014 *Nat. Commun.* **5** 5327
[49] Zambrana-Puyalto X, Vidal X and Molina-Terriza G 2014 *Nat. Commun.* **5** 4922
[50] Garoli D, Zilio P, Gorodetski Y, Tantussi F and De Angelis F 2016 *Sci. Rep.* **6** 29547
[51] Forbes K A 2020 *Phys. Rev. A* **105** 023524
[52] Milione G, Sztul H I, Nolan D A and Alfano R R 2011 *Phys. Rev. Lett.* **107** 053601
[53] Ren Z, Kong L, Li S, Qian S, Li Y, Tu C and Wang H 2015 *Opt. Express* **23** 26586
[54] Man Z, Dou X and Fu S 2019 *Opt. Lett.* **44** 427
[55] Man Z, Meng P and Fu S 2020 *Opt. Lett.* **45** 37
[56] Zhu M, Fu S and Man Z 2022 *Opt. Express* **30** 41048
[57] Zou C, Huang Q and Man Z 2023 *Opt. Commun.* **530** 129153
[58] Born M and Wolf E 1999 *Principles of Optics*, 7th edn. (Cambridge: Cambridge University Press) pp. 31–33
[59] Richards B and Wolf E 1959 *Proc. R. Soc. Lond. A* **253** 358
[60] Du L, Man Z, Zhang Y, Min C, Zhu S and Yuan X 2017 *Sci. Rep.* **7** 41001